



Phase relations of the Al_2O_3 – SiO_2 system at 13–21 GPa and 2300–2800 K and a new high-pressure $\text{Al}_2\text{Si}_2\text{O}_7$ phase

Youmo Zhou¹ · Tetsuo Irifune^{1,2} · Takahiro Kuribayashi³

Received: 7 February 2021 / Accepted: 5 June 2021 / Published online: 26 June 2021
© The Author(s), under exclusive licence to Springer-Verlag GmbH Germany, part of Springer Nature 2021

Abstract

Phase relations of the Al_2O_3 – SiO_2 system were determined by multi-anvil experiments at pressures of 13–21 GPa and temperatures of 2300–2800 K. We obtained a new high-pressure $\text{Al}_2\text{Si}_2\text{O}_7$ phase (227-phase), which possesses a triclinic unit cell ($Z=3$) with $a=7.0237(12)$ Å, $b=7.1002(14)$ Å, $c=6.6729(10)$ Å, $\alpha=103.466(15)^\circ$, $\beta=99.107(15)^\circ$, $\gamma=60.542(12)^\circ$, and $V=281.41(24)$ Å³, in addition to the two new high-pressure Al_2SiO_5 phases reported recently, kyanite II and kyanite III. Because of the formation of the three new phases at temperatures above 2400 K, the phase relations are complicated, in contrast to the previously-known phase assemblage of corundum + stishovite stable at the post-kyanite pressures and temperatures below 2400 K. The three new phases and also kyanite are chemically invariant intermediate phases in the binary system and can be formed by the isothermal reactions, Al_2O_3 (corundum) + SiO_2 (stishovite) = Al_2SiO_5 (kyanite II or III) and Al_2SiO_5 (kyanite, II, or III) + SiO_2 (stishovite) = $\text{Al}_2\text{Si}_2\text{O}_7$ (227-phase). In comparison to kyanite II and kyanite III, 227-phase is formed at higher temperatures. Crystal structure of 227-phase is based on distorted closest packing of O^{2-} and tetrahedrally- and octahedrally-coordinated cations, similar to those of kyanite and kyanite II. The appearance of 227-phase once again suggests the key effect of temperature for stabilizing dense crystal structures fully made of Al–O and Si–O polyhedra at high pressures.

Keywords Aluminum silicate · Al_2O_3 – SiO_2 binary system · Phase relation · Multi-anvil experiment

Introduction

Silicate is one of the most important mineral groups for many disciplines, such as materials and Earth science, and the various crystal structures of silicates and silica phases have been studied extensively and deeply, in which the Si–O polyhedra compose various frameworks, and Al^{3+} may replace a part of Si^{4+} on the frameworks (aluminosilicate) or occupy the cavities encircled by the frameworks (aluminum silicate). Recently we discovered two new high-pressure forms of Al_2SiO_5 by multi-anvil experiments at very high temperatures over 2400 K (Zhou et al. 2018). One is

stable at pressures of ~14–17 GPa, and the other is stable at ~17–23 GPa. Al_2SiO_5 is well known as the polymorphic minerals, andalusite, sillimanite, and kyanite (Ky). The two new Al_2SiO_5 phases are tentatively named kyanite II (Ky II) and kyanite III (Ky III), simply because the phase transitions of Al_2SiO_5 proceed in the sequence of Ky (< 14 GPa), Ky II (~14–17 GPa), and Ky III (> 17 GPa), with increasing pressure at temperatures above 2400 K (Zhou et al. 2018). On the other hand, Ky is stable up to ~13 GPa below 2400 K and decomposes into corundum (Cor) and stishovite (St) at higher pressures (e.g., Irifune et al. 1995).

Meanwhile we determined the crystal structures of Ky II and Ky III using single-crystal X-ray diffraction (SC-XRD) and reported the preliminary structural information (Zhou et al. 2018). Both are based on distorted closest packing of O^{2-} . In fact, this structural feature is common among many well-known related phases stable at high pressures. The examples are Ky (Winter and Ghose 1979), Cor (Tsuchiya et al. 2005), St, CaCl_2 -type SiO_2 , α - PbO_2 -type SiO_2 (Oganov et al. 2005), $\text{Al}_2\text{SiO}_4(\text{OH})_2$ Topaz-OH (Wunder et al. 1993), $\text{AlSiO}_3(\text{OH})$ phase Egg (Schmidt et al. 1998), MgSiO_3

✉ Youmo Zhou
zhouyoumo201637@gmail.com

¹ Geodynamics Research Center, Ehime University, Matsuyama, Ehime 790-8577, Japan
² Earth-Life Science Institute, Tokyo Institute of Technology, Meguro, Tokyo 152-8550, Japan
³ Department of Earth Science, Graduate School of Science, Tohoku University, Sendai, Tohoku 980-8578, Japan

akimotoite (Horiuchi et al. 1982), Mg_2SiO_4 forsterite, wadsleyite, and ringwoodite (Hazen 1976; Horiuchi and Sawamoto 1981; Sasaki et al. 1982). Therefore, the crystal structures of Ky II and Ky III again indicate that the polyhedral sites in the array of closest packed O^{2-} are suitable for Al^{3+} and Si^{4+} at high pressures.

However, there has been no solid theoretical or experimental evidence for the existence of new aluminum silicates at the post-Ky pressures, until we found Ky II and Ky III. On the contrary, from the simple viewpoint of crystallography of ionic crystals, the crystal structures of such phases should be unstable, and the instability factors can be the violation of the Pauling's 2nd principle, the structural distortion which results from the dimensional mismatch between Al–O and Si–O polyhedra, and the strong electrostatic repulsion caused by the dense packing of highly-charged but small-volume Al^{3+} and Si^{4+} . For example, Ky III has a V_3O_5 -like structure (e.g., Åsbrink 1980) made of Al–O and Si–O octahedra (Zhou et al. 2018), which agrees with the theoretical prediction made by Oganov and Brodholt (2000). Nevertheless, this theoretical study also pointed out the fact that no Al_2O_3 – SiO_2 compound with only sixfold coordination cations can satisfy the Pauling's 2nd principle, and therefore suggested the distortion of the crystal structure of V_3O_5 -like Al_2SiO_5 (i.e., Ky III) for the satisfaction of the bond-valence model (Brown 1992). Moreover, a completely-ordered cation arrangement was suggested by Oganov and Brodholt (2000) for the Ky III structure, that Al^{3+} and Si^{4+} occupy the face-sharing and non-face-sharing octahedral sites, respectively, to avoid stronger cation–cation repulsion which occurs when Si^{4+} occupies the face-sharing sites.

In comparison to most of the well-known high-pressure silicates and oxides, Ky II and Ky III are thermodynamically stable only at very high temperatures over 2400 K. Therefore, the effect of temperature should be key for stabilizing the crystal structures of Ky II and Ky III at high pressures. Besides the plausible explanation that Ky II and Ky III with higher configuration entropies are stabilized at higher temperatures, relative to the mixture of Cor and St, it is also likely that the crystal structures of Ky II and Ky III undergo sufficient expansion at very high temperatures, so that the cation–cation repulsion which destabilizes the crystal structures can be weakened effectively.

Many previous studies focused on the structural evolution and phase relations of Al_2O_3 and SiO_2 upon compression (e.g., Tsuchiya et al. 2004, 2005; Oganov et al. 2005; Oganov and Ono 2005). In contrast, nearly nothing has been known about the binary system at high pressures and temperatures. Our findings of Ky II and Ky III suggest the important temperature effect on both the crystal structures and phase relations involved in the binary system at high pressures. Therefore, it will be worthwhile to study the binary system under vast pressure–temperature conditions

and to look for unknown crystal structures and phase relations. On the basis of our recent study on Al_2SiO_5 , we further investigated the phase relations of the Al_2O_3 – SiO_2 system and found the third new high-pressure phase, in addition to Ky II and Ky III. This new phase has an $\text{Al}_2\text{Si}_2\text{O}_7$ chemical composition, and therefore it is tentatively named 227-phase. Here we show the high-pressure phase relations of the Al_2O_3 – SiO_2 binary system and discuss the stabilities of the new phases.

Experimental and analytical methods

A series of starting compositions were used: Al_4SiO_8 ($\text{Cor}_{67}\text{Qtz}_{33}$; Qtz = quartz), Al_2SiO_5 , $\text{Al}_4\text{Si}_3\text{O}_{12}$ ($\text{Cor}_{40}\text{Qtz}_{60}$), $\text{Al}_2\text{Si}_2\text{O}_7$ ($\text{Cor}_{33}\text{Qtz}_{67}$), and $\text{Al}_2\text{Si}_3\text{O}_9$ ($\text{Cor}_{25}\text{Qtz}_{75}$). Three kinds of starting materials were prepared. (1) Except for Al_2SiO_5 , the other starting compositions were prepared by mixing Cor and Qtz powders in the respective molar ratios. (2) The oxide mixtures, $\text{Cor}_{40}\text{Qtz}_{60}$, $\text{Cor}_{33}\text{Qtz}_{67}$, and $\text{Cor}_{25}\text{Qtz}_{75}$, were heated in a furnace at 2000 K for 1 h and then were cooled down in the air, and the fired products were ground into powders for use. (3) Single-phase Ky was synthesized at ~8 GPa and ~1700 K using a mixture of Cor and Qtz (1:1, molar ratio), and then it was ground into powders and was used as Al_2SiO_5 . Similarly, a mixture of Cor and Ky ($\text{Cor}_{50}\text{Ky}_{50}$) was synthesized from $\text{Cor}_{67}\text{Qtz}_{33}$ and was used as the reference to $\text{Cor}_{67}\text{Qtz}_{33}$ to check whether the chemical compositions of Cor in the final products were influenced by the kinetic effect.

The high-pressure products always contain more or less unreacted phases, when using the unfired oxide mixtures as the starting materials. The purpose of using the fired oxide mixtures is to facilitate the reactions, because they contain amorphous and intermediate phases (Text S1 and Fig. S1), which may be better precursors than Cor and Qtz. Using the fired $\text{Cor}_{33}\text{Qtz}_{67}$, nearly pure 227-phase has been synthesized. But unfortunately, the problem of incomplete reaction could not be fully solved by using the fired oxide mixtures, as shown later.

Experimental runs were performed with a Kawai-type multi-anvil apparatus at pressures of 13–21 GPa and temperatures of 2300–2800 K. Depending on the target temperatures, the durations were changed within 15–120 min. Tungsten carbide anvils with 4-mm truncations and Co-doped MgO octahedra with 10-mm edge lengths were used for pressure generation, and tubular LaCrO_3 heaters were used for temperature generation. The high-pressure cell contains two rhenium (Re) sample capsules with the thermocouple junction in between. Pressure calibrations were performed at high temperatures of 1873 and 2273 K, and heating temperatures were monitored by a W_{97}Re_3 – $\text{W}_{75}\text{Re}_{25}$ thermocouple. No correction was applied for the pressure effect on the

electromotive force of thermocouple. Details of the pressure calibrations and the temperature measurements can be found in the supplementary materials of Zhou et al. (2018). The uncertainties in pressure and temperature were estimated to be ± 1 GPa and ± 50 – 75 K, respectively. The temperature uncertainty involves the effect of thermal gradient, which is expected to be limited (Text S2). In each run, the high-pressure cell was first squeezed slowly, until the target load was reached. Then the temperature was increased to the target value at a rate of ~ 100 K/min and was kept constant under the fixed press load. After the duration of constant heating, the products were quenched to room temperature by shutting down the power supply and were obtained after decompression. The experimental conditions and results are shown in Table 1.

The products were embedded in epoxy resin and were polished for the subsequent analyses. Phase identification was made with a micro-focus XRD device (Rigaku Micro-Max-007HF) using Cu K α radiation. Figure S2 shows the XRD patterns of some typical products. The products were coated with carbon and were observed in a field-emission scanning electron microscope (FESEM, JEOL JSM7000F) under the working condition of 15 kV and 1 nA. Chemical compositions of the observed phases (Table S1) were analyzed with an energy-dispersive X-ray spectrometer (Oxford, Instruments X-Max^N). The quantification standards for Al and Si were Cor and Qtz, respectively.

A single-crystal fragment of 227-phase ($0.08 \times 0.04 \times 0.04$ mm³) was carefully selected using a polarized optical microscope for determining its crystal structure by SC-XRD. The measurement was performed with an automated four-circle X-ray diffractometer (Rigaku AFC-7S) operated at 50 kV and 30 mA, using monochromatized Mo K α radiation ($\lambda = 0.71073$ Å). To check the quality of the single-crystal sample and to collect the X-ray intensity data, synchrotron SC-XRD experiments ($\lambda = 0.70116$ Å) were also performed at BL-10A, PF, KEK, Japan (PAC. 2018G118; 2020G586). The initial atomic coordinate was set up using the charge flipping method (Palatinus and Chapuis 2007), and then was refined using the software SHELXL97 (Sheldrick and Schneider 1997) with the suite WinGX (Farrugia 1999). Details of the structural analyses on 227-phase will be reported in a separate work.

Results

Product textures and phase chemical compositions

Figures 1, 2, and 3 and Fig. S3 and S4 show the back-scattered electron images and elemental mappings of the products obtained under various pressure–temperature conditions. It is difficult to see contrast between different phases

(except Re) in the back-scattered electron images, while the elemental mappings highlight the distribution and dimension of each phase. Most of the products mainly consist of large (~ 5 – 50 μ m), euhedral grains. Triple junctions can be found between grains in almost all the products.

Table S1 shows the chemical compositions of all the observed phases, except those of fine-grained ($< \sim 5$ μ m) phases, which were not measured. Ky, Ky II, and Ky III have the same chemical composition of Al₂SiO₅, and 227-phase is chemically Al₂Si₂O₇. For both chemical compositions, the relative uncertainties in Al and Si numbers are up to $\sim 1\%$. These four phases were recovered as the intermediate phases with invariable chemical compositions. In other words, no obvious solid-solution reactions occurred on these four phases. In the obtained multi-phase assemblages, St is nearly pure SiO₂ in composition, while Cor contains substantial SiO₂ components up to 32 mol %, which is discussed later. Most of the Cor grains are chemically homogeneous, with the uncertainties of $\pm \sim 1$ mol % in the SiO₂ contents (Table 2).

As mentioned above, a few experimental runs were performed at 15.5 and 21 GPa around 2400 K using Cor₆₇Qtz₃₃ and Cor₅₀Ky₅₀ to check whether the chemical compositions of Cor in the high-pressure products were influenced by the kinetic effect. For examples, in the runs OS3383 and OS3395 (Table 1), both starting materials transformed into the same phase assemblage of Cor + St, but via different reactions. The chemical discrepancy of Cor between the two products of the same run is up to ~ 2 mol % in the SiO₂ content (Table 2), and this value is poorly indicative of a strong kinetic effect. Such comparison experiments were performed only around 2400 K, since the kinetic effect should be much weaker at higher temperatures.

Phase relations of the Al₂O₃–SiO₂ system

Figure 4 shows the composition–temperature phase diagrams of the Al₂O₃–SiO₂ system at different pressures. The preliminary experiments were conducted at 17 GPa using the unfired oxide mixtures, and the experimental results are shown in Fig. 4c. Cor₆₇Qtz₃₃, Cor₃₃Qtz₆₇, and Cor₂₅Qtz₇₅ transformed into Cor and St at temperatures below 2400 K (Fig. S3c). Cor₆₇Qtz₃₃ transformed into Cor and Ky III at 2373–2600 K (Fig. 1a and Fig. S2e), and the solubility of SiO₂ in Cor increases from ~ 4 to ~ 32 mol % with increasing temperature from 2300 to 2623 K. Cor₃₃Qtz₆₇ transformed into Ky III and St at 2473 K (Fig. 1b and Fig. S2f) and further into Ky III, 227-phase, and St at 2600–2723 K (Fig. 1c). All these experimental results suggest two isothermal reactions, Al₂O₃ (Cor) + SiO₂ (St) = Al₂SiO₅ (Ky III) and Al₂SiO₅ (Ky III) + SiO₂ (St) = Al₂Si₂O₇ (227-phase). Figure 1c shows a reaction-rim texture that 227-phase is in touch with Ky III and St, while Ky III and St are not in

Table 1 Experimental conditions and results

Run no	<i>P</i> (GPa)	<i>T</i> (K)	<i>t</i> (min)	Starting material	Product
OS3433	13	2273	120	Cor	Cor
				Cor ₃₃ Qtz ₆₇ Fired	Ky, St, tr. Cor
OS3400	13	2473	60	Cor ₃₃ Qtz ₆₇ Fired	Ky, 227-phase, St
OS3455	13	2623	20	Cor ₆₇ Qtz ₃₃	Cor, Ky
				Cor ₃₃ Qtz ₆₇ Fired	227-phase, tr. Ky
OS3360	15.5	2373	120	Cor ₃₃ Qtz ₆₇ Fired	Cor, St
				Cor ₂₅ Qtz ₇₅ Fired	Cor, St
OS3383	15.5	2373	90	Cor ₆₇ Qtz ₃₃	Cor, St
				Cor ₅₀ Ky ₅₀	Cor, St
OS3371	15.5	2400	60	Cor ₄₀ Qtz ₆₀ Fired	Ky II, 227-phase, St
				Cor ₂₅ Qtz ₇₅ Fired	Ky II, 227-phase, St
OS3346	15.5	2473	60	Ky	Ky II
				Cor ₃₃ Qtz ₆₇ Fired	227-phase
OS3384	15.5	2473	60	Cor ₆₇ Qtz ₃₃	Cor, Ky II
				Cor ₅₀ Ky ₅₀	Cor, Ky II
OS3354	15.5	2500	60	Cor ₃₃ Qtz ₆₇ Fired	227-phase, tr. St
				Cor ₂₅ Qtz ₇₅ Fired	Ky II, 227-phase, St
OS3387	17	2300	120	Cor ₆₇ Qtz ₃₃	Cor, St
				Cor ₂₅ Qtz ₇₅ Fired	Cor, St
OS3328	17	2373	120	Cor ₆₇ Qtz ₃₃	Ky III, Cor, tr. St
				Cor ₃₃ Qtz ₆₇	Cor, St
OS3333	17	2373	90	Ky	Ky III
				Cor ₂₅ Qtz ₇₅	Cor, St
OS3393	17	2400	90	Cor ₄₀ Qtz ₆₀ Fired	Cor, St
				Cor ₂₅ Qtz ₇₅ Fired	Cor, St
OS3325	17	2473	60	Cor ₆₇ Qtz ₃₃	Ky III, Cor, tr. St
				Cor ₃₃ Qtz ₆₇	Ky III, St, tr. Cor
OS3388	17	2473	60	Cor ₄₀ Qtz ₆₀ Fired	Ky III, St
				Cor ₂₅ Qtz ₇₅ Fired	Ky III, St
OS3353	17	2573	40	Cor ₃₃ Qtz ₆₇ Fired	Ky III, 227-phase, St
				Cor ₂₅ Qtz ₇₅ Fired	Ky III, St
OS3319	17	2600	40	Cor ₆₇ Qtz ₃₃	Cor, Ky III, tr. St
				Cor ₃₃ Qtz ₆₇	Ky III, 227-phase, tr. St
OS3324	17	2623	30	Cor ₆₇ Qtz ₃₃	Cor
				Cor ₃₃ Qtz ₆₇	Ky III, 227-phase, tr. Cor, tr. St
OS3373*	17	2623	30	Cor ₄₀ Qtz ₆₀ Fired	Ky II, 227-phase, tr. St
				Cor ₂₅ Qtz ₇₅ Fired	227-phase, St
OS3507	17	2650	45	Cor ₄₀ Qtz ₆₀ Fired	Ky III, 227-phase, tr. St
				Cor ₂₅ Qtz ₇₅ Fired	Ky III, St
OS3332	17	2673	40	Ky	Ky III
				Cor ₂₅ Qtz ₇₅	Ky III, St
OS3339	17	2723	30	Ky	Ky III
				Cor ₃₃ Qtz ₆₇	Ky III, 227-phase, St
OS3459	18	2623	15	Cor ₃₃ Qtz ₆₇ Fired	Ky III, St
OS3413	19	2900	30	Cor ₄₀ Qtz ₆₀ Fired	Ky III, St
				Cor ₂₅ Qtz ₇₅ Fired	Ky III, St
OS3395	21	2473	60	Cor ₆₇ Qtz ₃₃	Cor, St
				Cor ₅₀ Ky ₅₀	Cor, St
OS3467	21	2573	60	Cor ₆₇ Qtz ₃₃	Cor, St, tr. Ky III
				Cor ₃₃ Qtz ₆₇ Fired	Ky III, St, tr. Cor
OS3396	21	2673	30	Cor ₄₀ Qtz ₆₀ Fired	Ky III, St, tr. Cor
				Cor ₂₅ Qtz ₇₅ Fired	Ky III, St
OS3403	21	2773	20	Cor ₄₀ Qtz ₆₀ Fired	Ky III, St
				Cor ₂₅ Qtz ₇₅ Fired	Ky III, St

tr trace*The Al₂SiO₅ phase in the product of the fired Cor₄₀Qtz₆₀ was confirmed to be Ky II by XRD

touch with each other. This texture also suggests the isothermal reaction of the formation of 227-phase and further implies the existence of phase regions of Ky III + 227-phase and 227-phase + St within the Al_2SiO_5 – $\text{Al}_2\text{Si}_2\text{O}_7$ and $\text{Al}_2\text{Si}_2\text{O}_7$ – SiO_2 sub-systems, respectively. However, at 2673 K, $\text{Cor}_{25}\text{Qtz}_{75}$ transformed into Ky III and St, but 227-phase and St should have occurred instead.

The fired oxide mixtures were used in another set of experimental runs at the same pressure of 17 GPa, and the experimental results are also shown in Fig. 4c. Ky III and 227-phase dominantly occurred from the fired $\text{Cor}_{40}\text{Qtz}_{60}$ at 2650 K (Fig. 1d), which confirms the phase region of Ky III + 227-phase within the Al_2SiO_5 – $\text{Al}_2\text{Si}_2\text{O}_7$ sub-system. However, at the same temperature, the fired $\text{Cor}_{25}\text{Qtz}_{75}$ transformed into Ky III and St, but not 227-phase and St. A similar contradiction occurs between the products of the fired $\text{Cor}_{33}\text{Qtz}_{67}$ and $\text{Cor}_{25}\text{Qtz}_{75}$ at 2573 K. It is unclear why 227-phase could occur from the starting materials of $\text{Al}_4\text{Si}_3\text{O}_{12}$ and $\text{Al}_2\text{Si}_2\text{O}_7$, but not from those of $\text{Al}_2\text{Si}_3\text{O}_9$, under the same pressure–temperature conditions. In the run OS3373 (Table 1), only 227-phase and St occurred from the fired $\text{Cor}_{25}\text{Qtz}_{75}$ (Fig. 1e and Fig. S2g), but in the other capsule, Ky II, not Ky III, was confirmed in addition to 227-phase and St, which suggests that the actual pressure of this run should be at the lower side to the stability field of Ky III. Both the fired $\text{Cor}_{40}\text{Qtz}_{60}$ and $\text{Cor}_{25}\text{Qtz}_{75}$ transformed into Ky III and St at 2473 K and into Cor and St at and below 2400 K (Fig. S3d). On the basis of the experimental results of the unfired and fired oxide mixtures, two sets of isothermal phase boundaries can be roughly determined, and they agree with each other, within the uncertainty in temperature. At 17 GPa, Ky III and 227-phase occur at temperatures over ~2400 and ~2550 K, respectively.

The fired oxide mixtures were used instead of the unfired oxide mixtures for the Al_2SiO_5 – SiO_2 sub-system at 13, 15.5, and 21 GPa, and for the Al_2O_3 – Al_2SiO_5 sub-system, $\text{Cor}_{67}\text{Qtz}_{33}$ and $\text{Cor}_{50}\text{Ky}_{50}$ were used at the same pressures (Table 1). Figure 4b shows the phase diagram of the Al_2O_3 – SiO_2 system at 15.5 GPa, which is in shape similar to that of 17 GPa, while Ky II is stabilized at the lower pressure. At 2373 K, Cor and St occurred from $\text{Cor}_{67}\text{Qtz}_{33}$, $\text{Cor}_{50}\text{Ky}_{50}$, the fired $\text{Cor}_{33}\text{Qtz}_{67}$, and the fired $\text{Cor}_{25}\text{Qtz}_{75}$ (Figs. S3a, b). Both $\text{Cor}_{67}\text{Qtz}_{33}$ and $\text{Cor}_{50}\text{Ky}_{50}$ transformed into Cor and Ky II at 2473 K (Fig. 2a and Fig. S2d). Both the fired $\text{Cor}_{40}\text{Qtz}_{60}$ and $\text{Cor}_{25}\text{Qtz}_{75}$ transformed into Ky II, 227-phase, and St at 2400 K (Figs. 2b, c), and the clear difference in phase proportion should be mainly attributed to the different starting materials. The fired $\text{Cor}_{25}\text{Qtz}_{75}$ transformed into Ky II, 227-phase, and St at 2500 K (Fig. 2d). The fired $\text{Cor}_{33}\text{Qtz}_{67}$ transformed into nearly pure 227-phase at 2473 and 2500 K (Fig. S4c). Figures 2b–d show that 227-phase is in touch with Ky II and St, while Ky II and St are not in touch with each other. These textures suggest an isothermal

reaction, Al_2SiO_5 (Ky II) + SiO_2 (St) = $\text{Al}_2\text{Si}_2\text{O}_7$ (227-phase), and also imply the existence of phase regions of Ky II + 227-phase and 227-phase + St within the Al_2SiO_5 – $\text{Al}_2\text{Si}_2\text{O}_7$ and $\text{Al}_2\text{Si}_2\text{O}_7$ – SiO_2 sub-systems, respectively.

Cor and St occurred in a wide composition range between Al_2O_3 and SiO_2 at 15.5 GPa and 2373 K, while with slightly increasing temperature to 2400 K, both Ky II and 227-phase occurred from the fired $\text{Cor}_{40}\text{Qtz}_{60}$ and $\text{Cor}_{25}\text{Qtz}_{75}$, which suggests that the stability fields of Ky II and 227-phase have similar lower bounds near 2400 K. To satisfy the Gibbs phase rule, the phase region of Ky II + St should exist, which is narrow in temperature and is located between the phase region of Cor + St and those of Ky II + 227-phase and 227-phase + St, although we did not recover the phase assemblage of Ky II + St. At 15.5 GPa, the formation temperature of 227-phase should be slightly higher than that of Ky II near 2400 K.

Figure 4a shows the phase diagram of the Al_2O_3 – SiO_2 system at 13 GPa. At this pressure and above 2200 K, Ky is stable, and Cor and St cannot coexist with each other. $\text{Cor}_{67}\text{Qtz}_{33}$ transformed into Cor and Ky at 2623 K (Fig. 3a and Fig. S2b). Phase segregation can be found, but neither Cor nor Ky shows a melting texture. The fired $\text{Cor}_{33}\text{Qtz}_{67}$ transformed into Ky and St at 2273 K (Fig. 3b and Fig. S2c), into Ky, 227-phase, and St at 2473 K (Fig. 3c), and further into a product made of coarse-grained 227-phase and a few Ky inclusions at 2623 K (Fig. 3d). These phase transitions of the fired $\text{Cor}_{33}\text{Qtz}_{67}$ suggest an isothermal reaction, Al_2SiO_5 (Ky) + SiO_2 (St) = $\text{Al}_2\text{Si}_2\text{O}_7$ (227-phase). It can be noticed in Fig. 3c that Ky, 227-phase, and St are in touch with each other, which probably indicates the thermodynamic equilibrium between 227-phase and Ky + St. Therefore, it is concluded that at 13 GPa, 227-phase occurs at temperatures over 2473 K. The texture shown in Fig. 3c also implies the existence of phase regions of Ky + 227-phase and 227-phase + St within the Al_2SiO_5 – $\text{Al}_2\text{Si}_2\text{O}_7$ and $\text{Al}_2\text{Si}_2\text{O}_7$ – SiO_2 sub-systems, respectively.

Figure 4d shows the phase diagram of the Al_2O_3 – SiO_2 system at 21 GPa. Both $\text{Cor}_{67}\text{Qtz}_{33}$ and $\text{Cor}_{50}\text{Ky}_{50}$ transformed into Cor and St below 2600 K (Figs. S2a, S3e, f). Ky III and St occurred from the fired $\text{Cor}_{33}\text{Qtz}_{67}$ at 2573 K and from the fired $\text{Cor}_{40}\text{Qtz}_{60}$ and $\text{Cor}_{25}\text{Qtz}_{75}$ at 2673 and 2773 K. No 227-phase occurred within the Al_2SiO_5 – SiO_2 sub-system. Two additional runs were performed at 18 GPa, 2623 K and 19 GPa, 2900 K (Table 1). In both runs, Ky III and St occurred within the Al_2SiO_5 – SiO_2 sub-system.

Phase relations of $\text{Al}_2\text{Si}_2\text{O}_7$

Figure 5 shows the pressure–temperature phase diagram of $\text{Al}_2\text{Si}_2\text{O}_7$, and that of Al_2SiO_5 (Zhou et al. 2018) is also shown for comparison. The phase assemblage of Ky + St is stable for $\text{Al}_2\text{Si}_2\text{O}_7$ below ~14 GPa and ~2473 K. With the

Fig. 1 Back-scattered electron images and elemental mappings of the products obtained at 17 GPa. **a** OS3319, $\text{Cor}_{67}\text{Qtz}_{33}$. **b** OS3325, $\text{Cor}_{33}\text{Qtz}_{67}$. **c** OS3339, $\text{Cor}_{33}\text{Qtz}_{67}$. **d** OS3507, $\text{Cor}_{40}\text{Qtz}_{60}$ Fired. **e** OS3373, $\text{Cor}_{25}\text{Qtz}_{75}$ Fired

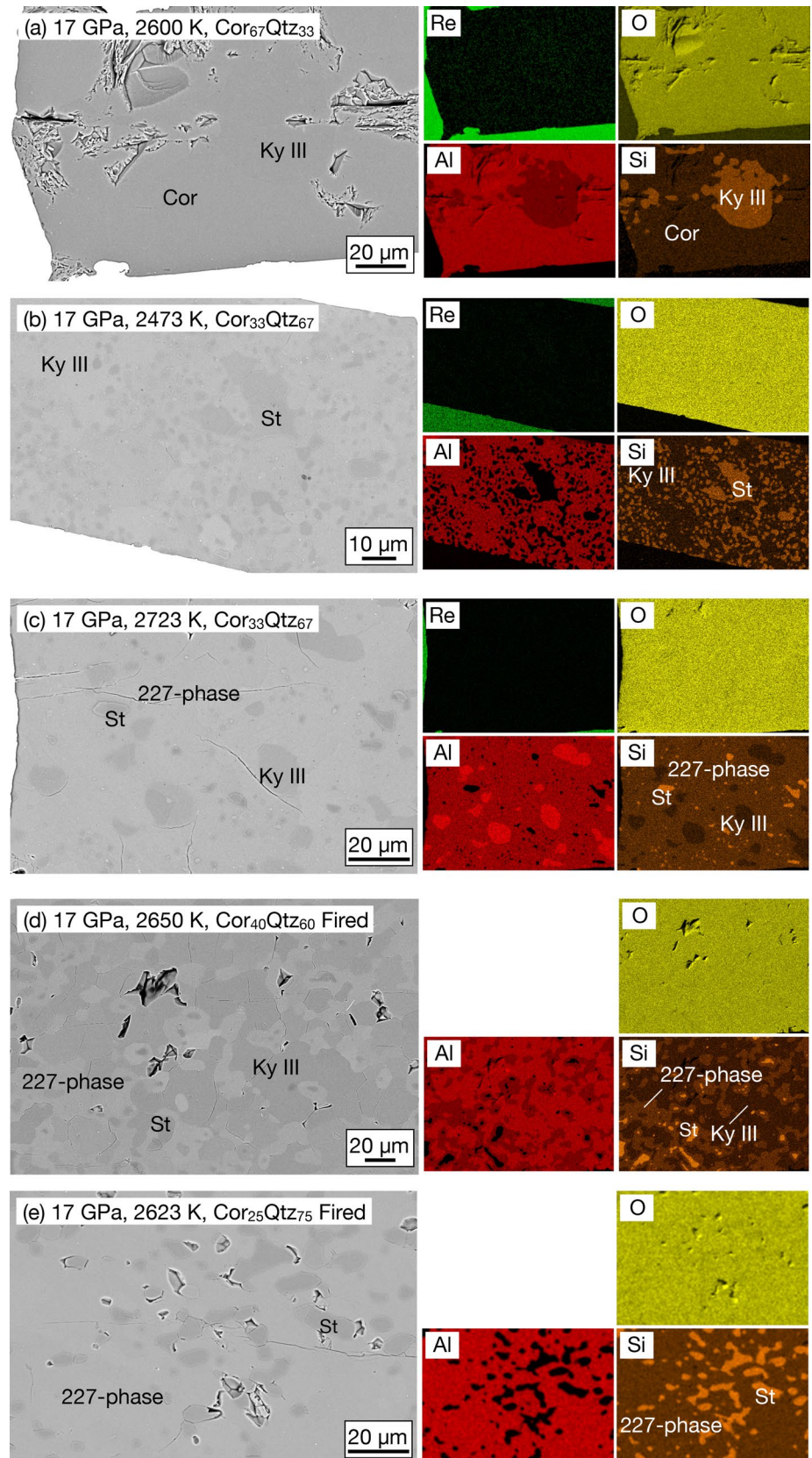
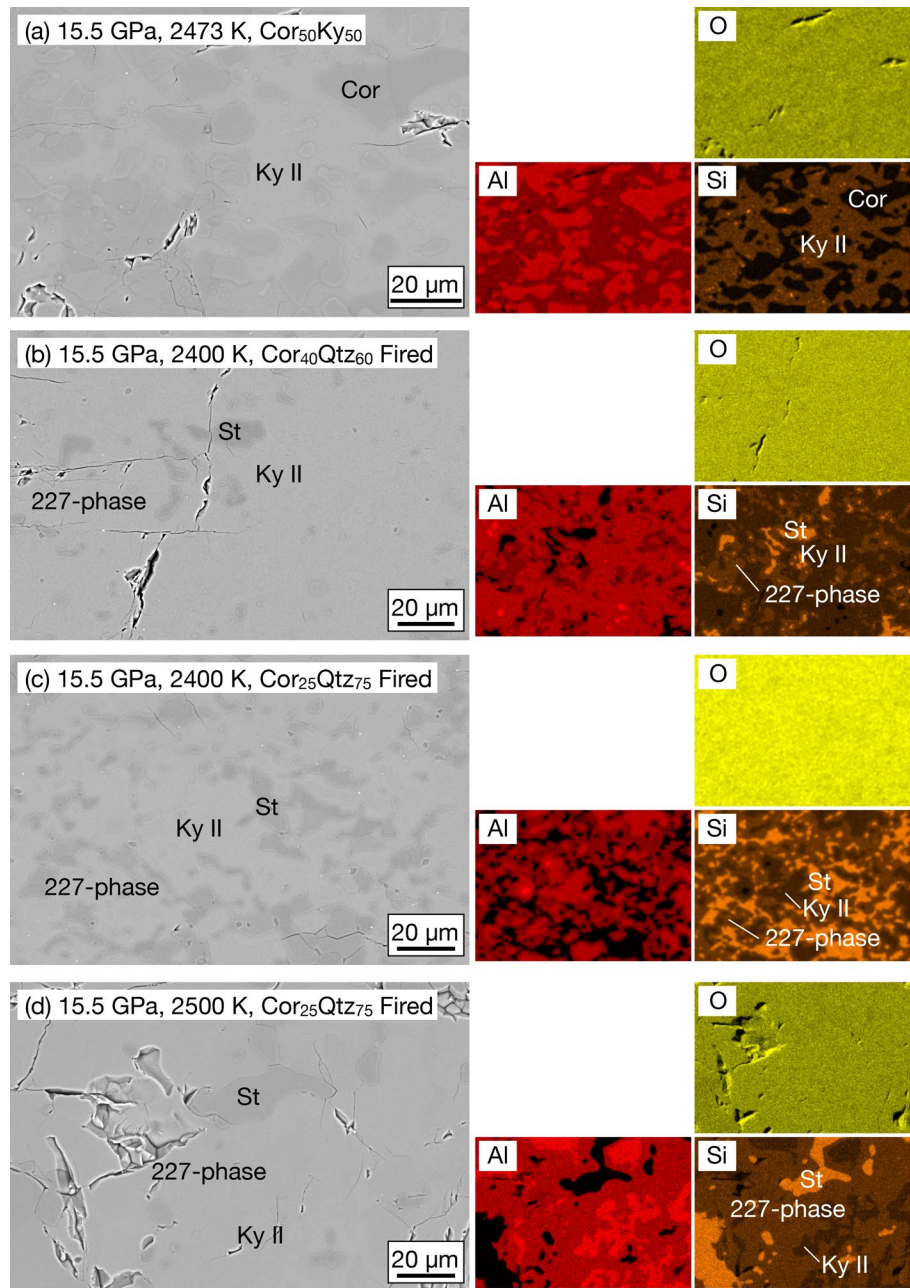


Fig. 2 Back-scattered electron images and elemental mappings of the products obtained at 15.5 GPa. **a** OS3384, $\text{Cor}_{50}\text{Ky}_{50}$. **b** OS3371, $\text{Cor}_{40}\text{Qtz}_{60}$ Fired. **c** OS3371, $\text{Cor}_{25}\text{Qtz}_{75}$ Fired. **d** OS3354, $\text{Cor}_{25}\text{Qtz}_{75}$ Fired

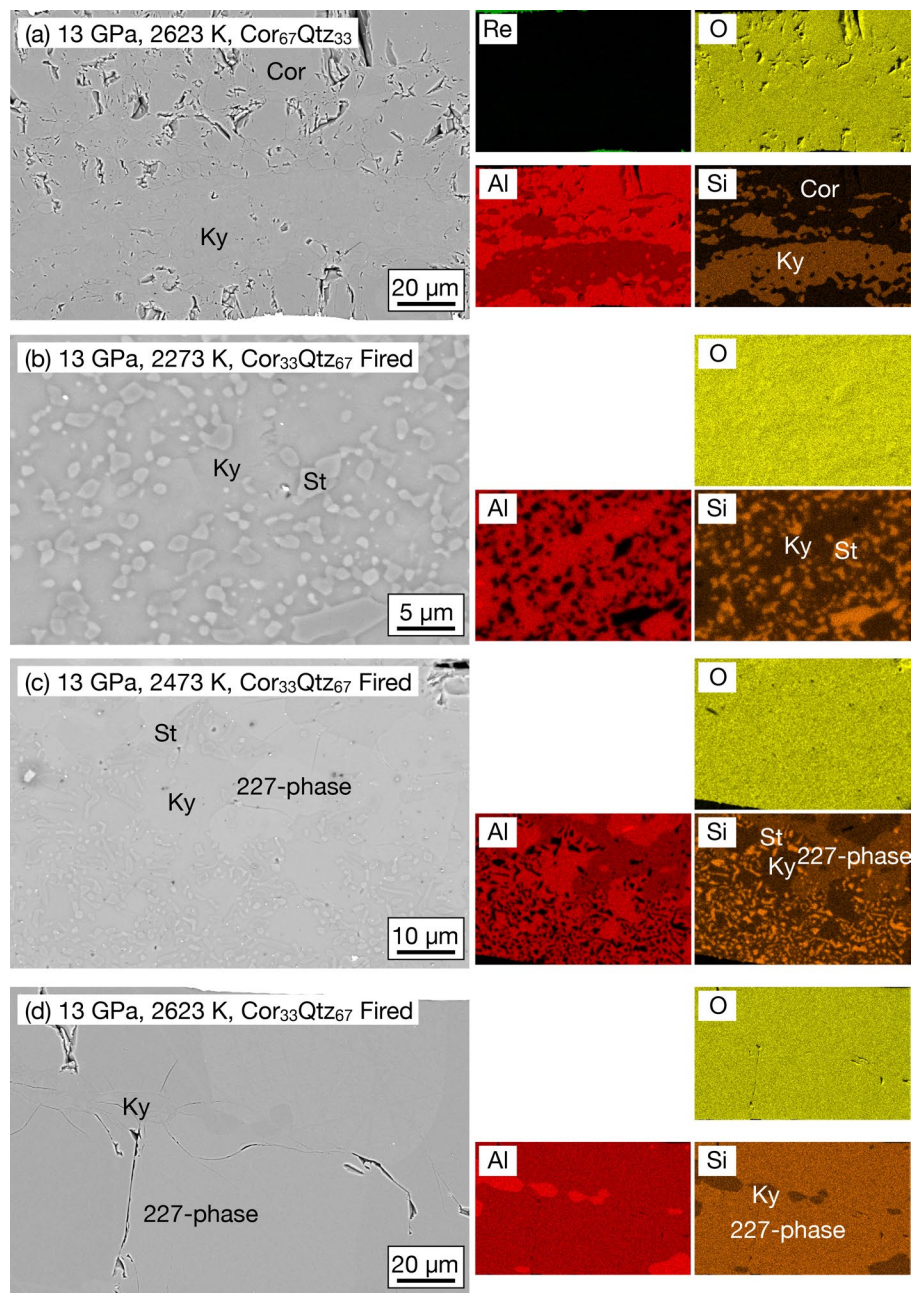


decomposition of Ky into Cor and St at $\sim 13\text{--}14$ GPa and below ~ 2400 K, the phase assemblage of Cor + St is stable for $\text{Al}_2\text{Si}_2\text{O}_7$ at higher pressures. Above ~ 2400 K, with the phase transitions of Al_2SiO_5 from Ky into Ky II near 14 GPa and further from Ky II into Ky III near 17 GPa, the phase assemblage of $\text{Al}_2\text{Si}_2\text{O}_7$ changes from Ky + St into Ky II + St and further from Ky II + St into Ky III + St. At 17 GPa, the stability field of Ky III + St is within $\sim 2400\text{--}2550$ K, and that of Ky II + St is expected to be much narrower at 15.5 GPa. 227-phase is stable at $\sim 13\text{--}17$ GPa and at the higher-temperature side adjacent to the stability fields of Ky/Ky II/Ky III + St. The formation temperatures of Ky II and Ky III

determined by the present study are consistent with those reported by Zhou et al. (2018).

Except for the phase boundary between Ky and Cor + St, of which the Clapeyron slope has been determined previously (e.g., Irifune et al. 1995), the other phase boundaries were qualitatively determined, based on both the experimental results and the contrasts between the ambient-pressure densities of the phase assemblages. As mentioned later, among the phase assemblages of $\text{Al}_2\text{Si}_2\text{O}_7$, 227-phase is denser than Ky/Ky II + St, but less dense than Ky III + St, and Cor + St is the densest; among the phase assemblages of Al_2SiO_5 , Cor + St is also the densest, and Ky III, Ky II,

Fig. 3 Back-scattered electron images and elemental mappings of the products obtained at 13 GPa. **a** OS3455, $\text{Cor}_{67}\text{Qtz}_{33}$. **b** OS3433, $\text{Cor}_{33}\text{Qtz}_{67}$ Fired. **c** OS3400, $\text{Cor}_{33}\text{Qtz}_{67}$ Fired. **d** OS3455, $\text{Cor}_{33}\text{Qtz}_{67}$ Fired



and Ky are the second, the third, and the fourth densest, respectively (Zhou et al. 2018). Knowing that the higher-temperature phases have larger entropies, the Clapeyron slopes of the phase boundaries can be qualitatively determined using the Clapeyron equation: $dP/dT = \Delta S/\Delta V$. To better determine the phase boundaries shown in Figs. 4 and 5, both forward and reverse reactions need to be studied by higher-quality experiments.

New high-pressure $\text{Al}_2\text{Si}_2\text{O}_7$ phase

227-phase occurred as a single phase or constituent of multi-phase assemblages from various starting materials at various pressures and temperatures. The structural and chemical analyses show that all the obtained 227-phase is identical in both crystal structure (Fig. 6 and Fig. S2g) and chemical composition (Table S1). Furthermore, 227-phase has been repeatedly synthesized using the starting materials in two distinct forms. All these results indicate that 227-phase occurred as thermodynamically stable phase in its stability field. On the other hand, almost all the products containing

Table 2 Unit cell parameters and unit cell volumes of corundum in function of the SiO₂ content

SiO ₂ Content (mol %)	<i>a</i> (Å)	<i>c</i> (Å)	<i>V</i> (Å ³)	Run no	Starting material
0	4.7582(8)	12.9952(20)	254.800(92)	OS3433	Cor
4.3(5)	4.7531(1)	12.9856(5)	254.068(17)	OS3387	Cor ₆₇ Qtz ₃₃
8.4(17)	4.7454(2)	12.9837(9)	253.207(39)	OS3360	Cor ₃₃ Qtz ₆₇ Fired
8.8(5)	4.7449(1)	12.9918(5)	253.314(21)	OS3383	Cor ₅₀ Ky ₅₀
9.7(7)	4.7422(3)	12.9849(12)	252.886(56)	OS3360	Cor ₂₅ Qtz ₇₅ Fired
10.5(5)	4.7430(1)	12.9961(11)	253.192(25)	OS3395	Cor ₅₀ Ky ₅₀
10.7(6)	4.7416(1)	12.9936(6)	252.994(26)	OS3383	Cor ₆₇ Qtz ₃₃
12.2(3)	4.7391(1)	12.9954(14)	252.766(30)	OS3395	Cor ₆₇ Qtz ₃₃
12.6(4)	4.7402(4)	12.9954(19)	252.878(54)	OS3328	Cor ₃₃ Qtz ₆₇
13.4(7)	4.7390(4)	13.0075(30)	252.989(72)	OS3333	Cor ₂₅ Qtz ₇₅
13.8(8)	4.7349(7)	13.0108(10)	252.609(45)	OS3328	Cor ₆₇ Qtz ₃₃
15.8(4)	4.7339(6)	13.0115(14)	252.517(65)	OS3325	Cor ₆₇ Qtz ₃₃
16.0(6)	4.7276(5)	13.0001(38)	251.630(92)	OS3467	Cor ₆₇ Qtz ₃₃
19.8(4)	4.7197(4)	13.0339(13)	251.443(45)	OS3319	Cor ₆₇ Qtz ₃₃
31.7(11)	4.6933(8)	13.0870(21)	249.650(96)	OS3324	Cor ₆₇ Qtz ₃₃

227-phase also contain unreacted phases. This should be mainly attributed to the kinetic effect.

The structural analysis on 227-phase by SC-XRD suggested a triclinic symmetry with unit cell parameters: $a = 7.0237(12)$ Å, $b = 7.1002(14)$ Å, $c = 6.6729(10)$ Å, $\alpha = 103.466(15)^\circ$, $\beta = 99.107(15)^\circ$, $\gamma = 60.542(12)^\circ$, and $V = 281.41(24)$ Å³. The space group is suggested to be $P 1$ (No. 2). The XRD pattern of polycrystalline 227-phase fits well with the crystal structure of 227-phase determined by SC-XRD (Fig. 6). Table S2 shows the observed and calculated d -spacing values of 227-phase.

Figure 7 shows the crystal structure of 227-phase. It is based on distorted closest packing of O²⁻ and tetrahedrally- and octahedrally-coordinated cations, similar to the crystal structures of Ky (Winter and Ghose 1979) and Ky II (Zhou et al. 2018). This similarity in cation coordination is in accordance with the fact that the stability field of 227-phase overlaps with those of Ky and Ky II in pressure. For Ky, Al³⁺ and Si⁴⁺ occupy the octahedral and tetrahedral sites, respectively. For Ky II and 227-phase, the number of tetrahedral sites is limited. Therefore, if the tetrahedral sites are preferred by Si⁴⁺, Si⁴⁺ has to occupy the octahedral sites as well. For Ky III, the higher-pressure phase, its crystal structure has only octahedrally-coordinated cations (Zhou et al. 2018). Now we cannot definitely decide the cation arrangements in the crystal structures of Ky II, Ky III, and 227-phase. The ordered configuration shown in Fig. 7 is temporary but can satisfy the chemical formula of 227-phase. However, a disordered configuration is expected, because of the high-temperature stability of 227-phase. More details of the crystal structure of 227-phase will be given in a separate work.

Using the equation $\rho = MZ/(N_A V)$, in which ρ is density, M is molecular weight, Z is the number of formula units in a unit cell, N_A is the Avogadro constant, and V is unit cell volume, the density of each phase can be calculated, and then that of each phase assemblage can be calculated. The unit cell volumes of Cor, St, and Ky were taken from Kirfel and Eichhorn (1990), Yamanaka et al. (2002), and Winter and Ghose (1979), respectively, and those of Ky II and Ky III were taken from Zhou et al. (2018). For the phase assemblages of Al₂Si₂O₇, the calculation results are $\rho_{\text{Cor+St}} = 4.069$ g/cm³, $\rho_{\text{Ky+St}} = 3.750$ g/cm³, $\rho_{\text{KyII+St}} = 3.917$ g/cm³, $\rho_{\text{KyIII+St}} = 4.026$ g/cm³, and $\rho_{\text{227-phase}} = 3.932(3)$ g/cm³ ($Z = 3$).

Schmidt et al. (1997) reported that a mixture of 36 mol % Ky, 29 mol % Cor, and 35 mol % St transformed into a mixture of Cor and an Al₂Si₂O₇ phase at 18 GPa and ~2773 K. This pressure–temperature condition is close to the stability field of 227-phase. Therefore, the previous Al₂Si₂O₇ phase is probably the same as 227-phase. However, in the previous study, 227-phase was suggested to be a breakdown product of Ky, which is contradicted by our experimental results. We observed no decomposition of Ky, Ky II, or Ky III in the stability field of 227-phase, while they occurred as single phases (Figs. S4a, b, and Fig. 4; Zhou et al. 2018). Taking our results for reference, it is possible that the reactions between Cor/Ky (III) and St yielded 227-phase in the previous study, because the starting material was a mixture of Ky, Cor, and St, not pure Ky. But even so, the coexistence of Cor and 227-phase should be thermodynamically metastable. Otherwise, there is another possibility that Ky, Ky II, or Ky III does decompose into Cor and 227-phase, as suggested by the previous study, but at further higher temperatures, while such conditions were not achieved in the present study.

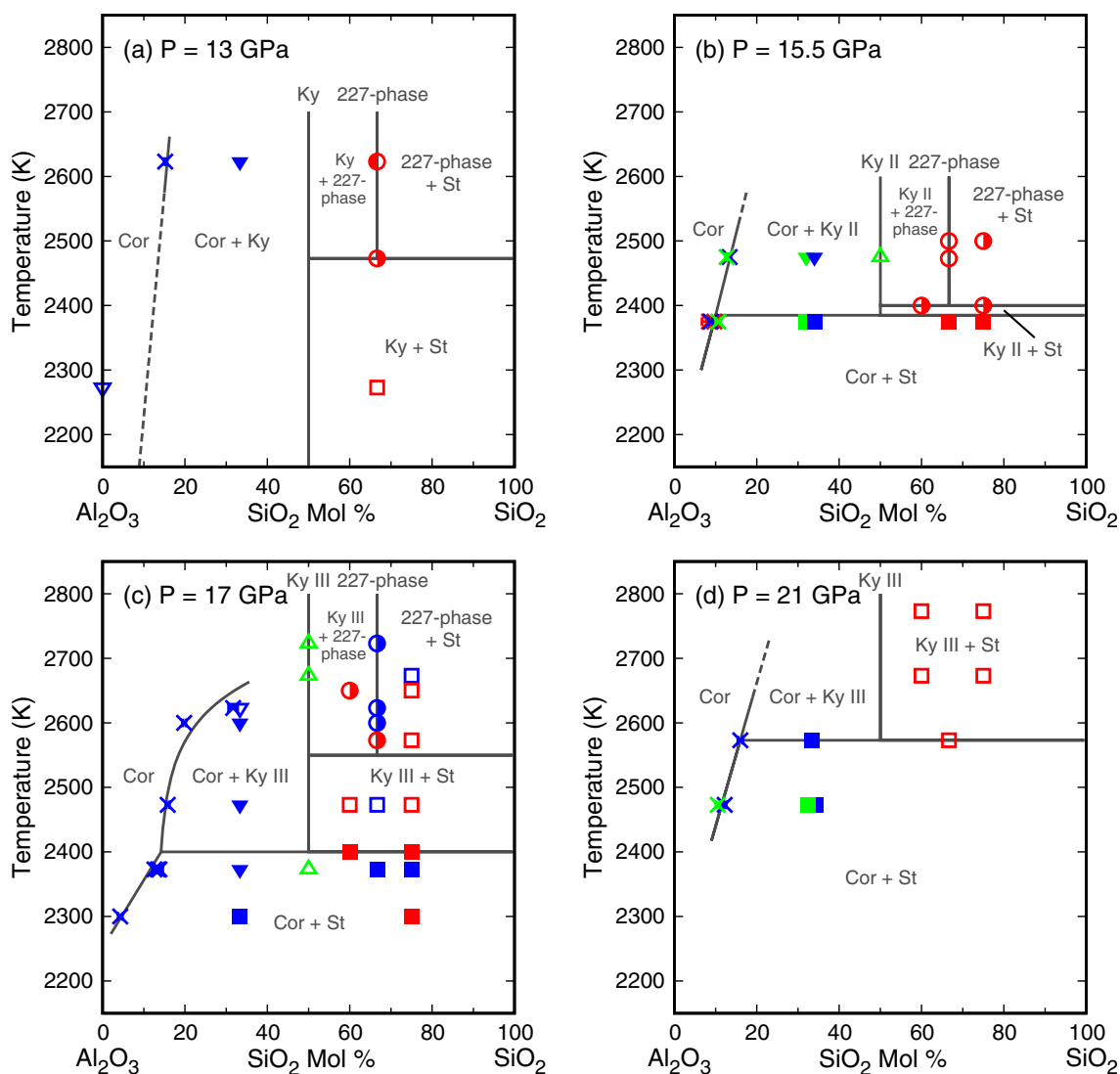


Fig. 4 Phase diagrams of the Al_2O_3 – SiO_2 system at **a** 13 GPa, **b** 15.5 GPa, **c** 17 GPa, and **d** 21 GPa. The colors, blue, red, and green, are used to distinguish the phase assemblages synthesized using the three kinds of starting materials, unfired oxide mixtures, fired oxide mixtures, and the Ky-containing materials, respectively. The cross symbols represent the SiO_2 contents in Cor. The solid lower-triangles represent Cor + Ky/Ky II/Ky III. The hollow lower-triangles represent

Cor. The hollow upper-triangles represent Ky II or Ky III. The circle with filled left half represents Ky + 227-phase. The hollow circles represent 227-phase. The circles with filled right half represent Ky/Ky II/Ky III + 227-phase + St. The hollow squares represent Ky/Ky II/Ky III + St. The solid squares represent Cor + St. The phase boundaries showing the Al_2O_3 solubility in St are quite close to the right borders

Ahmed-Zaïd and Madon (1991) reported that some Al_2SiO_5 or $\text{Al}_2\text{Si}_2\text{O}_7$ phases were formed after heating Ky, anorthite, grossular, and pyrope in a diamond anvil cell at 40–70 GPa and 2500 K. However, these previous results have not yet been reproduced by any other studies, and the previous Al_2SiO_5 phase structurally differs from Ky II and Ky III (Zhou et al. 2018). As for 227-phase and the previous $\text{Al}_2\text{Si}_2\text{O}_7$ phase, they should have different crystal structures, because the synthesis pressures are different and the latter should not have tetrahedrally-coordinated cations. In addition, no other $\text{Al}_2\text{Si}_2\text{O}_7$ polymorph has been known so far, except an amorphous isochemical phase called metakaolin,

which can be derived from the dehydration of kaolin clay at the ambient pressure (e.g., Inoue and Yamaguchi 2003).

Corundum containing SiO_2

Cor in the multi-phase assemblages contains substantial SiO_2 components (Table S1). The SiO_2 solubility in Cor shows a positive temperature dependence, and the pressure dependence needs to be further studied. This solubility can be used as the pressure and temperature indicator for high-pressure experiments. Compared with the common indicators of pressure and temperature, such as the

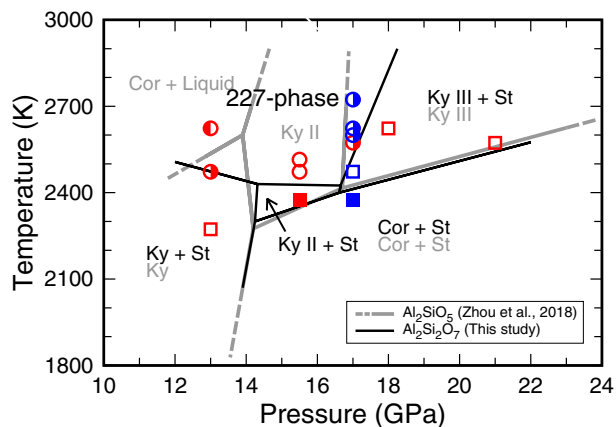


Fig. 5 Phase diagram of $\text{Al}_2\text{Si}_2\text{O}_7$. The two colors, blue and red, are used to distinguish the phase assemblages synthesized using the two kinds of starting materials, the unfired and fired oxide mixtures, respectively. The phase boundaries for Al_2SiO_5 reported by Zhou et al. (2018) are shown for comparison. Some experimental results were also used to determine the phase boundaries for $\text{Al}_2\text{Si}_2\text{O}_7$, but they are not shown, because the starting compositions are different. The solid squares represent Cor + St. The hollow squares represent Ky/Ky III + St. The hollow circles represent 227-phase. The circle with filled left half represents Ky + 227-phase. The circles with filled right half represent Ky/Ky III + 227-phase + St

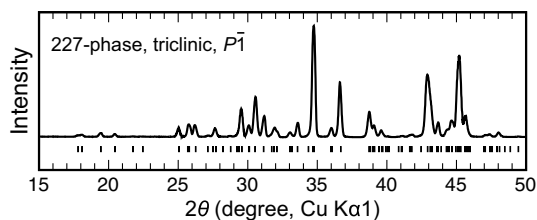


Fig. 6 XRD pattern of a polycrystalline single-phase sample of 227-phase (Run OS3346). The short bars beneath the profile denote the peak positions calculated based on the crystal structure of 227-phase determined by SC-XRD. Due to the large grain size of this sample, relative intensities of the observed peaks should deviate from those expected for a randomly-oriented polycrystalline sample

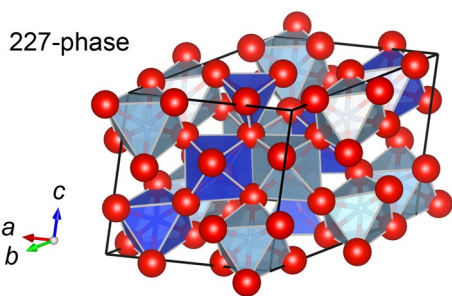


Fig. 7 Crystal structure of 227-phase. The red spheres represent approximately closest packed O^{2-} . The dark and light blue polyhedra are occupied by Si^{4+} and Al^{3+} , respectively. This ordered configuration is temporary, and the actual configuration is to be resolved

enstatite–diopside solid solutions, SiO_2 -containing Cor is thermodynamically stable in a much wider pressure–temperature space and in particular suitable for use at very high temperatures above 2300 K.

The incorporation of SiO_2 component in Cor obviously influences the unit cell parameters of Cor. Table 2 lists the unit cell parameters of Cor in function of the SiO_2 content, and these data are plotted in Fig. 8. The length of a axis and the unit cell volume linearly decrease with increasing the SiO_2 content. The length of c axis remains constant or slightly decreases with the SiO_2 content up to ~ 10 mol %, and then it linearly increases with further increasing the SiO_2 content. SiO_2 -free Cor was annealed at high pressure and temperature (OS3433, Table 1), and its unit cell parameters were obtained by XRD as well and are consistent with the reference data (Fig. 8), which suggests that the non-linear change in the length of c axis should be unlikely caused by the error of XRD analysis.

There is only one kind of cation site in the crystal structure of Cor, which is octahedrally-coordinated and shares a face with another octahedral site along c axis. The substitution of Si^{4+} for Al^{3+} causes the formation of cation vacancy for charge balance and stronger electrostatic repulsion between a pair of face-sharing cation sites filled by Al^{3+} and Si^{4+} , because Si^{4+} has a larger valence but a smaller ionic radius. Therefore, the shortening of a axis with increasing the SiO_2 content can be attributed to the fact that more Al^{3+} is replaced by smaller Si^{4+} , and more cation vacancies occur. The change in the length of c axis suggests that when the SiO_2 content is 0–10 mol %, the effects of smaller Si^{4+} and cation vacancy cancel out the effect of stronger Al^{3+} – Si^{4+} repulsion between a pair of face-sharing cation sites, and the latter effect becomes dominant with further increasing the SiO_2 content. As the integrated result of the changes in axis lengths, the unit cell volume decreases with increasing the SiO_2 content. In addition, we found no additional peaks for Cor in the XRD patterns, and therefore we suggest a disordered substitution of Si^{4+} for Al^{3+} in the crystal structure of Cor, which is in accordance with the very high experimental temperatures.

St containing Al_2O_3 component is another interesting issue. In the present study, the Al_2O_3 contents in St are ~ 0.5 – 1.8 wt % (Table S1). These values represent the Al_2O_3 solubilities in St at the corresponding pressures and temperatures. Our values are clearly lower than the Al_2O_3 capacity of hydrous St (e.g., up to ~ 8 wt %, as reported by Litasov et al. 2007). The higher Al_2O_3 capacity of hydrous St is likely attributed to the incorporation of hydrogen, although the Al/H ratios were larger than 1 and need to be further studied. In the case of dry St, the substitution of Al^{3+} for Si^{4+} has two possible mechanisms, the oxygen-vacancy-formation type and the interstitial- Al^{3+} type (e.g., Litasov et al. 2007). Both destabilize the crystal structure of

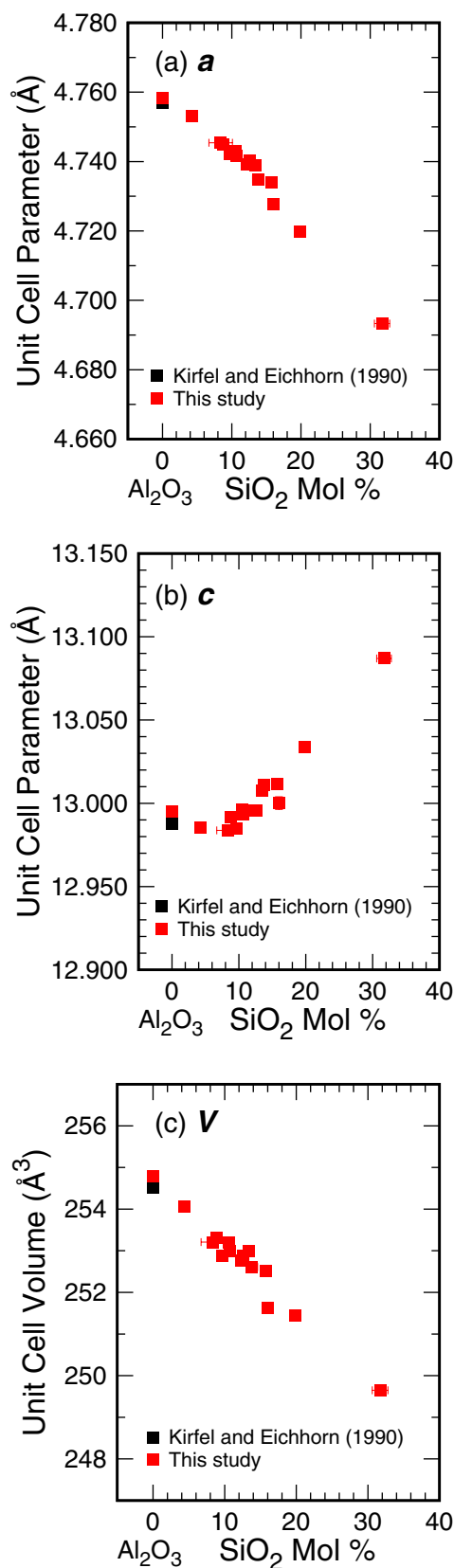


Fig. 8 Unit cell parameters and unit cell volumes of corundum in function of the SiO₂ content: **a** *a* axis; **b** *c* axis; **c** unit cell volume. Most of the horizontal and vertical error bars are covered by the square symbols

St, and the former is likely dominant. The formation of oxygen vacancy may destroy the oxygen framework (distorted closest packing) in the crystal structure of St. This explains the lower Al₂O₃ solubility of dry St. In contrast, in the case of SiO₂-containing Cor, the oxygen framework will not be destroyed by the formation of cation vacancy.

Discussion

We determined the phase relations of the Al₂O₃–SiO₂ system by multi-anvil experiments at 13–21 GPa and 2300–2800 K and found a new Al₂Si₂O₇ phase, which is the third new high-pressure phase recently found in the Al₂O₃–SiO₂ system. Similar to Ky II and Ky III, 227-phase is thermodynamically stable only at very high temperatures above ~2400 K, and therefore it unlikely exists in the Earth's mantle under the typical geotherms. Many phases in the Al₂O₃–SiO₂ system are structurally based on distorted closest packing of O²⁻, and the examples are Cor, St, CaCl₂-type SiO₂, α-PbO₂-type SiO₂, Ky, Ky II, and Ky III (Winter and Ghose 1979; Oganov et al. 2005; Tsuchiya et al. 2005; Zhou et al. 2018). Now 227-phase has become the latest example.

The finding of 227-phase further suggests the key effect of temperature for stabilizing dense crystal structures fully made of Al–O and Si–O polyhedra at high pressures, although such phases were previously expected to be unstable relative to the mixtures of Al₂O₃ and SiO₂ phases (Oganov and Brodholt 2000). The structural instability can be likely caused by the steric distortion (Brown 1992) and the cation–cation repulsion. The former factor is inevitable for the new phases, due to the closest packing of O²⁻ and the dimensional mismatch between Al–O and Si–O polyhedra. Nevertheless, the existence of the new phases implies that their crystal structures can satisfy the valence-sum rule (Brown 1992), and the probably large deviations from the valence-sum rule still do not exceed the tolerance limit, at least in the stability fields. On the other hand, no solid-solution reactions occurred on the new phases, which implies that much larger deviations caused by cation substitution and formation of cation or anion vacancy are not allowed.

Compared to the steric distortion, the cation–cation repulsion is likely the main factor that destabilizes the crystal structures of the new phases. This can be easily realized by considering the structural evolution of SiO₂ phases upon compression in the sequence of St, CaCl₂-type SiO₂, and α-PbO₂-type SiO₂ (Oganov et al. 2005). For examples, the relative incompressibility of *c* axis of St is caused by the cation–cation repulsion (Ross et al. 1990); the linkage of Si–O octahedra does not drastically change upon the phase transition from CaCl₂-type SiO₂ into α-PbO₂-type SiO₂, but the zigzag chains of edge-sharing octahedra in the crystal structure of α-PbO₂-type SiO₂ lead to stronger cation–cation

repulsion, relative to the straight chains of CaCl_2 -type SiO_2 , and therefore α - PbO_2 -type SiO_2 is stabilized at higher pressures; unlike Cor, no silicates or SiO_2 phases contain face-sharing octahedral sites filled by only Si^{4+} in the crystal structures.

Although in the crystal structures of the new phases, the Al^{3+} – Al^{3+} and Al^{3+} – Si^{4+} repulsion weaker than the Si^{4+} – Si^{4+} repulsion should be dominant, the cation packings are denser than those in the crystal structures of high-pressure SiO_2 phases, which may make the cation–cation repulsion the main threat to the stabilities of the new phases. In the V_3O_5 -like structure (Åsbrink 1980) of Ky III, 3/5 of the octahedral sites are filled by cations. For Ky II and 227-phase, the fill rates are $\sim 3/5$ and $\sim 4/7$, respectively. These values are close to 2/3 for Cor but higher than the value for St, (less than) 1/2. The extreme stability fields of the new phases suggest that pressure cannot alone stabilize these phases by overcoming the cation–cation repulsion, but at very high temperatures, their crystal structures may undergo sufficient expansion, so that the repulsion can be effectively weakened. A similar effect may work on SiO_2 -containing Cor, which explains the positive temperature dependence of the SiO_2 solubility in Cor.

The high-pressure phase relations of the Al_2O_3 – SiO_2 system are indeed more complicated than that represented by the mixture of Cor and St. It will be interesting to further study this binary system at higher pressures and temperatures, and more unknown crystal structures and phase relations may be found. In particular, unknown refractory hydrous phases, which are similar to our new phases structurally, may exist in the Al_2O_3 – SiO_2 – H_2O ternary system, because hydrogen is likely able to adjust the local bond-valence sum, without largely changing the crystal structures.

Summary

Phase relations of the Al_2O_3 – SiO_2 system were determined at pressures of 13–21 GPa and temperatures of 2300–2800 K. Three new phases (Ky II, Ky III, and 227-phase) can be formed as chemically invariable intermediate phases in the binary system at temperatures above 2400 K via the isothermal reactions, Al_2O_3 (Cor) + SiO_2 (St) = Al_2SiO_5 (Ky II or Ky III) and Al_2SiO_5 (Ky, Ky II, or Ky III) + SiO_2 (St) = $\text{Al}_2\text{Si}_2\text{O}_7$ (227-phase). The formation of 227-phase needs higher temperatures in comparison with that of Ky II and Ky III. At temperatures below 2400 K, the phase assemblage of Cor + St dominates the main composition range in the binary system at the post-Ky pressures. Cor can contain substantial SiO_2 components at high pressures and temperatures, and the solubility of SiO_2 component in Cor shows a positive temperature-dependence.

The extreme stability fields of the three new phases rule out their occurrence in the Earth's interior, but imply their unique stabilities at very high temperatures. Although the polyhedral sites in the array of closest packed O^{2-} are suitable for Al^{3+} and Si^{4+} at high pressures, dense crystal structures based on closest packing of O^{2-} and tetrahedrally- and octahedrally-coordinated Al^{3+} and Si^{4+} have never been confirmed until our recent and present findings. The appearance of 227-phase in addition to Ky II and Ky III again suggests the key effect of temperature for stabilizing dense crystal structures fully made of Al–O and Si–O polyhedra at high pressures. Since the cation–cation repulsion seems to be the main instability factor for the crystal structures of such phases, it may be weakened effectively at very high temperatures, due to thermal expansion. It is worthwhile to study the phase relations in the Al_2O_3 – SiO_2 and some related systems under unexplored pressure–temperature conditions and to look for more unknown crystal structures and phase relations.

Supplementary Information The online version contains supplementary material available at <https://doi.org/10.1007/s00269-021-01149-3>.

Acknowledgements The synchrotron X-ray diffraction experiments were performed at BL-10A, PF, KEK, Japan (PAC. 2018G118; 2020G586).

Funding The present study was supported by the Grand-in-Aid for Scientific Research on Innovative Areas (No. 15H5829) to Tetsuo Irifune.

Declarations

Conflict of interest The authors declare that they have no conflict of interest.

References

- Ahmed-Zaid I, Madon M (1991) A high-pressure form of Al_2SiO_5 as a possible host of aluminum in the lower mantle. *Nature* 353(6343):426–428. <https://doi.org/10.1038/353426a0>
- Åsbrink S (1980) The crystal structure of and valency distribution in the low-temperature modification of V_3O_5 . The decisive importance of a few very weak reflexions in a crystal-structure determination. *Acta Cryst B* 36:1332–1339. <https://doi.org/10.1107/S0567740880006036>
- Brown ID (1992) Chemical and steric constraints in inorganic solids. *Acta Cryst B* 48:553–572. <https://doi.org/10.1107/S0108768192002453>
- Farrugia LJ (1999) WinGX suite for small-molecule single-crystal crystallography. *J Appl Crystallogr* 32(4):837–838. <https://doi.org/10.1107/S0021889899006020>
- Hazen RM (1976) Effects of temperature and pressure on the crystal structure of forsterite. *American Mineralogist* 61:1280–1293. <https://pubs.geoscienceworld.org/msa/ammin/article-abstract/61/11-12/1280/40602/Effects-of-temperature-and-pressure-on-the-crystal?redirectedFrom=fulltext>
- Horiuchi H, Sawamoto H (1981) β - Mg_2SiO_4 : Single-crystal X-ray diffraction study. *American Mineralogist* 66:568–575. <https://pubs>

- [geoscienceworld.org/msa/ammin/article-abstract/66/5-6/568/41286/Mg2SiO4-Single-crystal-X-ray-diffraction-study?redirectedFrom=fulltext](https://pubs.geoscienceworld.org/msa/ammin/article-abstract/66/5-6/568/41286/Mg2SiO4-Single-crystal-X-ray-diffraction-study?redirectedFrom=fulltext)
- Horiuchi H, Hirano M, Ito E, Matsui Y (1982) MgSiO₃ (ilmenite-type): single crystal X-ray diffraction study. *American Mineralogist* 67:788–793. <https://pubs.geoscienceworld.org/msa/ammin/article-abstract/67/7-8/788/41416/MgSiO3-ilmenite-type-single-crystal-X-ray?redirectedFrom=fulltext>
- Inoue K, Yamaguchi A (2003) Synthesis of Al₄SiC₄. *J Am Ceram Soc* 86(6):1028–1030. <https://doi.org/10.1111/j.1151-2916.2003.tb03414.x>
- Irifune T, Kuroda K, Minagawa T, Unemoto M (1995) Experimental study of the decomposition of kyanite at high pressure and high temperature. In: Yukutake T (ed) *The Earth's central part: Its structure and dynamics*, Tokyo: Terra Scientific Publishing Company (TERRAPUB), pp 35–44. <https://www.terrpub.co.jp/e-library/ecp/pdf/EC0035.PDF>
- Kirfel A, Eichhorn K (1990) Accurate structure analysis with synchrotron radiation. The electron density in Al₂O₃ and Cu₂O. *Acta Cryst A* 46:271–284. <https://doi.org/10.1107/S0108767389012596>
- Litasov KD, Kagi H, Shatskiy A, Ohtani E, Lakshantov DL, Bass JD, Ito E (2007) High hydrogen solubility in Al-rich stishovite and water transport in the lower mantle. *Earth Planetary Sci Lett* 262:620–634. <https://doi.org/10.1016/j.epsl.2007.08.015>
- Oganov AR, Brodholt JP (2000) High-pressure phases in the Al₂SiO₅ system and the problem of aluminous phase in the Earth's lower mantle: ab initio calculation. *Phys Chem Miner* 27:430–439. <https://doi.org/10.1007/s002699900081>
- Oganov AR, Ono S (2005) The high-pressure phase of alumina and implications for Earth's D'' layer. *Proc Natl Acad Sci USA* 102:10828–10831. <https://doi.org/10.1073/pnas.0501800102>
- Oganov AR, Gillan MJ, David Price G (2005) Structural stability of silica at high pressures and temperatures. *Phys Rev B* 71:064104. <https://doi.org/10.1103/PhysRevB.71.064104>
- Palatinus L, Chapuis G (2007) Superflip—a computer program for the solution of crystal structures by charge flipping in arbitrary dimensions. *J Appl Crystallogr* 40(4):786–790. <https://doi.org/10.1107/S0021889807029238>
- Ross NL, Shu J, Hazen RM, Gasparik T (1990) High-pressure crystal chemistry of stishovite. *American Mineralogist* 75:739–747. <https://pubs.geoscienceworld.org/msa/ammin/article-abstract/75/7-8/739/42397/High-pressure-crystal-chemistry-of-stishovite?redirectedFrom=fulltext>
- Sasaki S, Prewitt CT, Sato Y, Ito E (1982) Single-crystal X-ray study of γ-Mg₂SiO₄. *J Geophys Res* 87:7829–7832. <https://doi.org/10.1029/JB087iB09p07829>
- Schmidt MW, Poli S, Comodi P, Zanazzi PF (1997) High-pressure behavior of kyanite: decomposition of kyanite into stishovite and corundum. *Am Miner* 82:460–466. <https://doi.org/10.2138/am-1997-5-603>
- Schmidt MW, Finger LW, Angel RJ, Dinnebier RE (1998) Synthesis, crystal structure, and phase relations of AlSiO₃OH, a high-pressure hydrous phase. *Am Miner* 83:881–888. <https://doi.org/10.2138/am-1998-7-820>
- Sheldrick GM, Schneider TR (1997) SHELXL: High-resolution refinement. *Methods Enzymol* 277:319–343. [https://doi.org/10.1016/S0076-6879\(97\)77018-6](https://doi.org/10.1016/S0076-6879(97)77018-6)
- Tsuchiya T, Caracas R, Tsuchiya J (2004) First principles determination of the phase boundaries of high-pressure polymorphs of silica. *Geophys Res Lett* 31:L11610. <https://doi.org/10.1029/2004GL019649>
- Tsuchiya J, Tsuchiya T, Wentzcovitch RM (2005) Transition from the Rh₂O₃(II)-to-CaIrO₃ structure and the high-pressure-temperature phase diagram of alumina. *Phys Rev B* 72:020103(R). <https://doi.org/10.1103/PhysRevB.72.020103>
- Winter JK, Ghose S (1979) Thermal expansion and high-temperature crystal chemistry of the Al₂SiO₅ polymorphs. *American Mineralogist* 64:573–586. https://www.minsocam.org/ammin/AM64/AM64_573.pdf
- Wunder B, Rubie DC, Ross II CR, Medenbach O, Seifert F, Schreyer W (1993) Synthesis, stability, and properties of Al₂SiO₄(OH)₂: a fully hydrated analogue of topaz. *American Mineralogist* 78:285–297. <https://pubs.geoscienceworld.org/msa/ammin/article-abstract/78/3-4/285/42731/Synthesis-stability-and-properties-of-Al2SiO4-OH-2?redirectedFrom=fulltext>
- Yamanaka T, Fukuda T, Tsuchiya J (2002) Bonding character of SiO₂ stishovite under high pressures up to 30 GPa. *Phys Chem Miner* 29(9):633–641. <https://doi.org/10.1007/s00269-002-0257-3>
- Zhou Y, Irifune T, Ohfuji H, Kuribayashi T (2018) New high-pressure forms of Al₂SiO₅. *Geophys Res Lett* 45:8167–8172. <https://doi.org/10.1029/2018GL078960>

Publisher's Note Springer Nature remains neutral with regard to jurisdictional claims in published maps and institutional affiliations.